Dome seeing analysis of the Anglo-Australian Telescope

Josephine Munro,[a],* **Jonah Hansen[ORCID],[a]** **Tony Travouillon[ORCID],[a]**
Doris Grosse,[a] **and Andrei Tokovinin[ORCID][b]**

[a]Australian National University, Research School of Astronomy and Astrophysics, Advanced Instrumentation and Technology Centre, Weston Creek, Australian Capital Territory, Australia

[b]Cerro Tololo Inter-American Observatory, NSF NOIRLab, La Serena, Chile

Abstract. Dome seeing is an often overlooked avenue for seeing improvement for a telescope. Because most existing telescope domes have not been characterized for turbulence, there is an opportunity to improve the overall seeing by minimizing the dome contribution, thereby optimizing scientific productivity and operations. A dome turbulence sensor has recorded data in the Anglo-Australian Telescope (AAT) over the past year. The instrument consists of a collimated laser beam that propagates (and double passes) between the AAT's primary mirror box and a flat mirror on the secondary strut. The angle-of-arrival fluctuations are used to derive a dome-seeing-proxy in arcsec. We found the dominant effects to be the temperature gradients and wind speed. Convection conditions are considerably more detrimental to the dome-seeing-proxy than thermal inversion conditions. Unlike other large telescopes, there is no discernible relationship between the dome-seeing-proxy and relative wind direction. Concerning telescope operations, it would be worth considering lowering the air-conditioning set point temperature to include a higher proportion of observations under thermal inversion. Nevertheless, this must be carefully weighed with the risk of condensation in the dome, a major concern for a site with frequent high relative humidity. © *The Authors. Published by SPIE under a Creative Commons Attribution 4.0 International License. Distribution or reproduction of this work in whole or in part requires full attribution of the original publication, including its DOI.* [DOI: 10.1117/1.JATIS.9.1.017004]

1 Introduction

1.1 Background

Optical turbulence in the atmosphere arises from inhomogeneous pockets of refractive index. These inhomogeneities are primarily caused by temperature gradients and are particularly variable at the boundary between different air velocities. The refractive index inhomogeneities result in a spatially dependent phase difference across a wavefront that evolves over time. For an imaging system, image degradation occurs when a phase difference is present across the pupil. There are a few quantitative values for characterizing the turbulence in the atmosphere, such as coherence length and coherence time.[1] One quantity often used is the "seeing," which is the angular full width-half maximum of the broadened image of an observed star. The seeing is effectively the resolution limit imposed by the turbulent atmosphere.

Optical telescope sites are chosen for natural good seeing and low light pollution. These are often remote sites at high altitudes. Sites with good seeing are also usually located near the coast or on an island with prevalent laminar ocean winds. The ocean surface is homogeneous compared to land, which has various levels of soil exposure, vegetation, buildings/structures, and uneven topography. Consequently, the air over the ocean is much more stable compared to the air over the land. Mauna Kea observatories in Hawaii,[2] Roque de los Muchachos Observatory

---

*Address all correspondence to Josephine Munro, josephine.munro@anu.edu.au

(La Palma) in the Canary Islands,[3] and Paranal Observatory in Chile[4] are all examples of sites with excellent natural seeing. The stratification of the atmosphere and its effect on seeing is generally well known, but slight differences that are unique to a site will occur due to the natural (and built) topography of the landscape and local weather patterns. This has driven the popularity of conducting site testing campaigns before a telescope is commissioned to ascertain the unique turbulence statistics of a particular site.[5]

The dome imparts a less well-known source of seeing degradation for a telescope. A dome structure protects sensitive, fragile equipment from external conditions, such as rain and debris carried by the wind. Wind also needs to be prevented from causing fluctuating deformation of the telescope structure and mirrors. These deformations due to wind pressure will cause a non-negligible amount of image degradation. Even though the dome protects the contents from these effects, it is also a source of turbulence that contributes to image degradation. First, how the dome interacts with the outside environment will impact the dome turbulence; for instance, more mechanical turbulence will enter the dome when the dome slit faces directly into the wind. Secondly, the thermal inertia of the dome creates temperature gradients, detrimentally affecting the dome turbulence. This is also the case for the telescope and all the equipment within a dome that will radiate heat. One of the main sources of this radiant heat is the primary mirror. Also of concern are instruments/electronics that produce heat when in operation. While thermal gradient dissipation and airflow throughout the dome cannot be eliminated, they can be optimised. Dome turbulence is now considered for new telescopes in their design stage with thermal and airflow control modeled before a structure is even built.[6]

1.2 Previous Dome Seeing Studies

Dome seeing has been considered since at least the late 70s.[7] Early research in this field mainly consisted of recording the seeing as seen through the telescope, but this measurement is entangled with atmospheric seeing and optical aberrations. Dedicated studies have only been employed relatively recently, leaving many telescopes already in operation with no data on their dome seeing that is fully disentangled from atmospheric seeing. In the absence of this data, many operational telescopes have aimed to minimize dome seeing by equalizing the temperature differences between the primary mirror and indoor and outdoor temperatures. There have been multiple dome seeing studies of currently operational domes built before dome seeing was carefully considered in the planning stage. These studies have led to substantial improvements in dome seeing for that telescope.

Salmon et al.[8] measured image quality in various bands on the 3.6-m Canada France Hawaii telescope (CFHT) between 2005 and 2008. They found that temperature differences, wind, and the dome slit direction relative to wind direction substantially affected image quality. They also discussed the relevance and impact of sensor errors, especially temperature recording errors. Additionally, Salmon et al. found that convection (when a lower level is warmer than a higher level) resulted in worse seeing compared to temperature inversions (when higher levels are warmer than lower levels) by an approximate factor of three, supporting that convective eddies are more turbulent than eddies found at thermal inversions.[8] They also quantified the image quality degradation contributions from optics and optomechanical imperfections and estimated the "observatory-free" site seeing. In this study, they used many temperature sensors situated in and around the telescope to fully understand the temperature gradients within the dome.

Simulations of the aerodynamic properties of existing telescope domes have also proved to be a fruitful venture in identifying areas of dome seeing improvement. Baril et al.[9] found that the traditional unvented hemispherical dome contributed significantly to the degradation of the very good natural seeing at the CFHT site. Without the option of using forced airflow through the dome (due to building constraints), Baril et al.[9] used water-tunnel modelling, wind-tunnel tests, and computational fluid dynamics modelling to support dome skin slit designs to encourage optimal mixing of inside and outside temperatures.

With the prevalence of non-Kolmogorov turbulence in the dome, a dedicated instrument is needed to disentangle the dome seeing from atmospheric seeing, as demonstrated by Lai et al.[10]

Lai et al.[10] characterized the C_n^2 found in the CHFT and showed a variation in the C_n^2 for different areas in the University of Hawaii 2.2-m telescope (UH88) tube with a particular focus on the stronger turbulence found closer to the primary mirror within the tube, which can be explained by uneven thermal stratification.

Bustos and Tokovonin[11] built and tested a dome seeing monitor that uses the angle-of-arrival of a laser beam to extract a dome seeing proxy. With this instrument, the median dome seeing was determined to be 0.2 arcsec for the Blanco telescope.[11]

Each of the studies mentioned above has confirmed the general understanding of dome turbulence: larger temperature gradients and higher wind speeds are more detrimental to the dome seeing. Their results also show that the individual conditions in a dome produce unique turbulence in that telescope. For example, the tube on the University of Hawaii 2.2-m telescope causes thermal stratification leading to a source of turbulence that is not a concern to other telescopes that do not share this design feature. Consequently, simulations or observational studies are needed to make conclusions about an individual telescope's dome seeing. Not only was the Anglo-Australian Telescope (AAT) commissioned before dome seeing was routinely considered in the planning stage, but it also has unique structural features that may impact the dome seeing.

1.3 AAT and the Dome Turbulence Sensor

The AAT is a 3.9-m optical telescope at Siding Spring Observatory (SSO), Coonabarabran, Australia. The AAT was commissioned in the 1970s and built to withstand the high winds at its location. The dome is a conventional hemisphere with a small dome slit. The dome slit, as well as being azimuthally constrained, has windscreens that close down from the top and up from the bottom to reduce the dome aperture to a minimum area to help combat the high wind conditions at SSO. The dome is air-conditioned to reduce the time required to thermally equilibrate the observatory and is reduced once the dome is open. There are fans that force air to mix in the mirror cell, but there is no dedicated cooling for the primary mirror. Vents located on the third floor (main floor level, southern side) eject cold air from the air-conditioning, where it circulates around the telescope and is collected by vents (control room floor, west and east sides) on the fourth floor to be recycled. Substantial permanent structures on the north and west sides of the dome prevent uniform air circulation.

A 2013 site characterisation study of SSO gave a median seeing value of 1.2 arcsec[12] and the seeing from the AAT is reported as 1.5 arcsec.[13] Several studies have contributed to the knowledge of the seeing conditions in the dome, both quantitative and qualitative. Dome seeing was significantly improved with the addition of two large fans to improve the thermal mixing in 1980.[14] One of the main sources of dome seeing has been identified as the primary mirror.[15] The most significant detrimental effect on dome seeing corresponds to when the primary is warmer than the surrounding indoor air, and there is little degradation of the dome seeing when the mirror is colder than the indoor air. Ryan and Wood[15] found that the seeing degraded over the course of the night; this was independent of the seasons. They also proposed that the dome seeing is unrelated to the dome slit temperature gradient. However, these previous studies of the dome turbulence at the AAT have had limited datasets of about 100 measurements[14] or substantial recording errors in the AAT's seeing measurement.[15] To fully characterise the AAT's dome turbulence, a dome turbulence sensor (DOTS) was installed to collect data over 89 nights, spanning from August 2021 to July 2022.

DOTS is an instrument based heavily on the dome seeing monitor used for the Blanco 4-m telescope.[11] To understand what causes changes in the dome seeing, we tested the correlation of the dome-seeing-proxy with meteorological parameters gathered by the observatory. These correlations were studied to identify optimum conditions, giving avenues to the observatory to operate under the lowest achievable seeing.

This paper will describe the DOTS instrument and the meteorology variables used for this study. An overview of the AAT dome seeing statistics and significant influences on the dome seeing is presented. Seasonal and hourly trends and any minor influences on the dome seeing are discussed. A summary of the results, conclusions, and future work are presented.

2 Data Acquisition

2.1 *DOTS Instrument*

DOTS measures the angle of arrival of a laser beam propagated between the primary box and secondary strut (reflected back by a flat mirror). The double root-mean-square (RMS) (double due to the double pass) of the angle-of-arrival of this relatively small column is not equal to the dome seeing but is a quantitative proxy that is relative to dome seeing. Fundamentally, because all interpretations of seeing are based on turbulence models and there are no turbulence models that adequately encapsulate the conditions in a dome, the double RMS will give us a relative understanding of the dome seeing fluctuations rather than an absolute quantitative measure. This is discussed well by Bustos and Tokovinin,[11] where it is shown that the measured dome-seeing-proxy by the absolute image motion monitor has a proportionality coefficient to the dome seeing on the order of one. Henceforth, we will describe the measurement made by DOTS as a dome-seeing-proxy.

DOTS consists of a breadboard section attached to the primary mirror box and a flat mirror attached to the inside surface of the secondary strut, probing a column of air between the primary and secondary mirrors of the telescope. This does mean we miss out on turbulence information between the top end and the dome slit, shown in simulations to be a significant source of turbulence.[5] Figure 1 is a photo of the AAT parked at zenith with labels showing the locations of the breadboard section of DOTS and the flat mirror. Figure 2 shows the optical layout of the instrument. A 35-mm-diameter collimated laser beam is propagated to the flat mirror, ~ 13 m away, and reflected back through the lenses $L1$ and $L2$, reflected by a beam splitter, and focused by $L3$ onto the camera. Focal spots that were non-Gaussian in shape were discarded from the
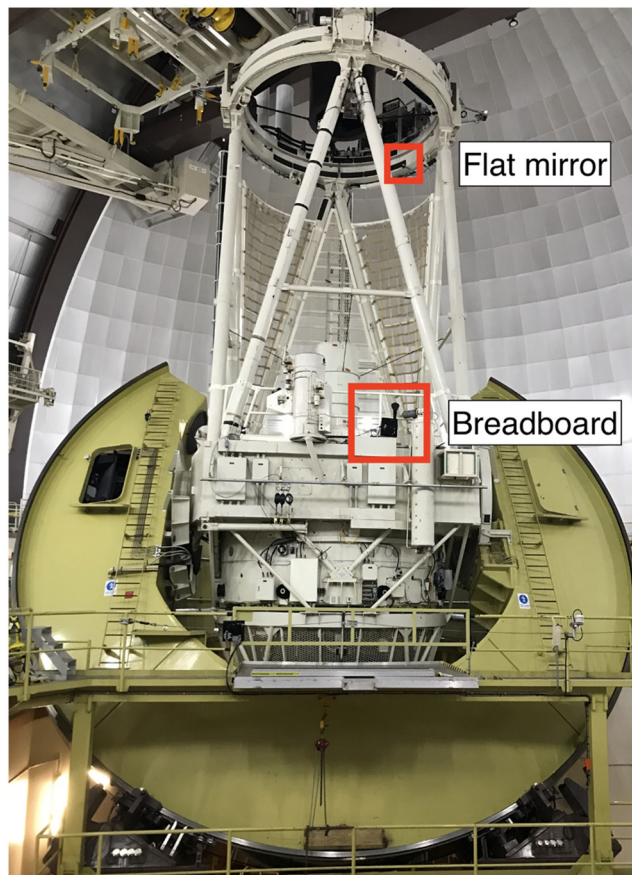

Fig. 1 Location of the breadboard section of DOTS and the flat mirror while the telescope is parked at zenith. Image credit: J. Munro.
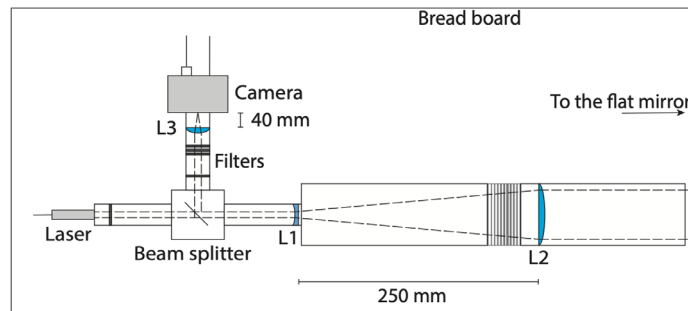
Fig. 2 DOTS optical layout of breadboard components. A 532-nm laser beam is expanded to 35 mm by the lens relay, propagated up to a flat mirror attached to the secondary strut, and reflected back through the relay to be focused onto a camera.

dataset; this was a very small fraction of the total dataset as the 35-mm beam is sufficiently small to avoid imaging a scintillated focal spot. The camera is a Prosilica GC 650 with a pixel size of 7.4 μm. The optics used for DOTS are not diffraction limited, where spherical aberration is the prominent aberration. The RMS radius of the focal spot is 45.62 μm. This results in an over-sampled spot size of 6.2 pixels. The pixel sampling can be improved to 2.5 to 3 pixels for future use of the instrument to increase the signal-to-noise ratio (SNR). The cheaper non diffraction-limited optics are adequate for this study as we use a 532-nm laser as a bright illumination source. The laser's intensity is reduced by neutral density filters so that the focal spot does not saturate the CCD.

The software for DOTS is based on that created by Bustos and Tokovinin.[11] The python script reduces the centroid position data to obtain the dome-seeing-proxy. The script accumulates the centroid position for 30 s with 40 frames per second and an exposure time of 20 ms to produce an RMS "seeing" value every 30 s.

DOTS captures data between 16- and 8-hr local time (UTC +10) each night as the telescope is operating. The analyzed dataset was further limited to when the dome was open. Even though there are still interesting interactions between temperature gradients within the dome when closed, we are primarily concerned about the open dome case as it represents the dome seeing conditions experienced during scientific observations. Nevertheless, our dataset does agree with Lai et al. that the dome seeing (proxy) is better when the dome is closed.[10] If an instrument is in use on the telescope that is sensitive to the 532-nm light from the DOTS laser diode module, DOTS is not switched on and does not collect data that night. The dataset consists of 89 nights, ranging over a year from August 2021 to July 2022, which is sufficient to cover the wide range of meteorological conditions across all four seasons in this year. The top graph of Fig. 3 shows our dataset with the bottom graph showing a closeup of four nights worth of data in late February 2022.

2.2 Vibrations

Expanding on the software used to calculate the dome-seeing-proxy, we have also introduced the use of the power spectrum of the centroid variance to extract vibration information, much in the same way it has been used for vibration mitigation for tip/tilt adaptive optics correction.[16,17] The power spectrum is fitted to the Kolmogorov power law with the caveat that since the turbulence in the dome is unlikely to be Kolmogorov in nature, the power index is allowed to float. Prominent vibrations will cause a peak in the power law, and so these peaks are identified, fitted to a Gaussian, and then removed from the original dataset to reduce the contamination of vibration in the dome-seeing-proxy. Figure 4(a) shows an example of the conducted lab tests, which shows the power spectrum with an induced vibration at 5 Hz measured to be 4.93 Hz. This is very close to representing zero turbulence as a very short optical path between the breadboard and the flat mirror was used. Figure 4(b) shows turbulence with no induced vibrations, and Fig. 4(c) shows turbulence with an induced vibration at 10 Hz. The fitting algorithm we are using has a limited ability to identify small amplitude vibrations that are difficult to distinguish
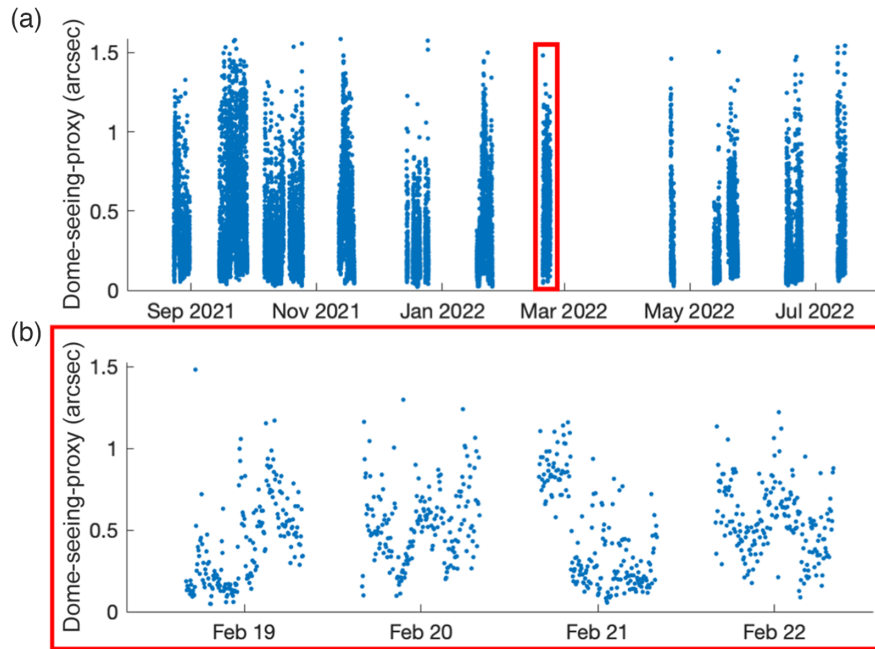
Fig. 3 (a) Dome-seeing-proxy over a year from August 2021 to July 2022. (b) Closeup of four consecutive nights of dome-seeing-proxy data in late February 2022. These plots show all data over the 16- to 08-hr time range.
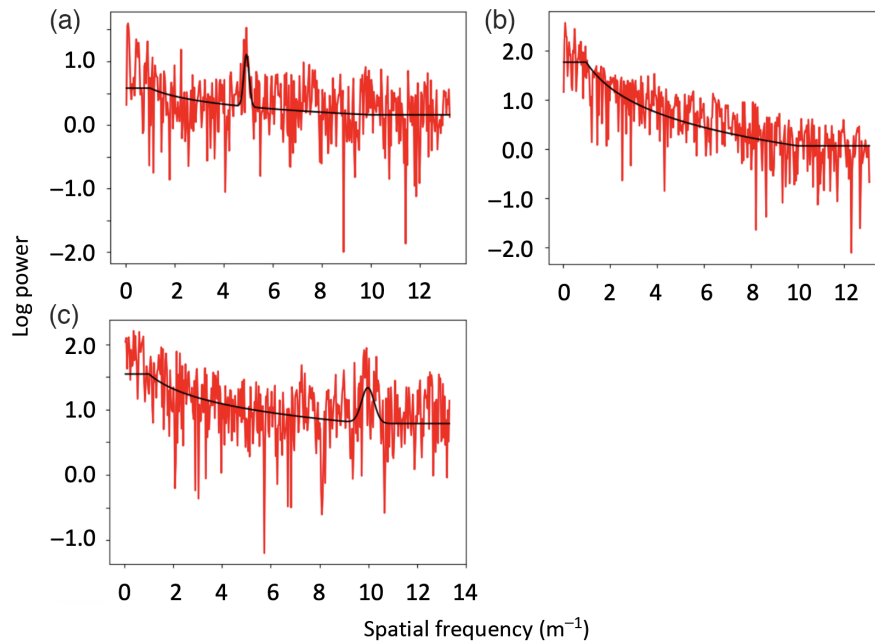

Fig. 4 (a) Power spectrum with a very small amount of turbulence and a known vibration at 5 Hz, measured to be 4.93 Hz, (b) power spectrum with induced turbulence and no vibrations, and (c) power spectrum with induced turbulence and a known vibration at 10 Hz.

from background noise. This is likely to cause a small positive bias in our dome-seeing-proxy measurement. This bias is proportional to turbulence strength, resulting in higher amplitude vibrations being unidentifiable in strong turbulence conditions. The maximum observable frequency is limited to half the sampling rate. Because our sampling rate is 40 Hz, our maximum observable vibration frequency is 20 Hz. The relatively low sampling rate is used to reduce the
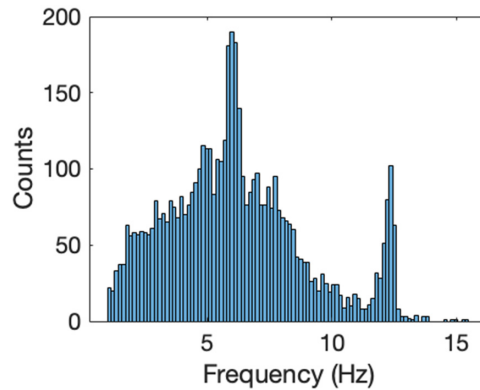
Fig. 5 Frequency histogram of vibrations. A primary peak is seen at 6 Hz and a secondary peak at 12 Hz.

bias of the undetected vibrations since the signal in the power spectrum related to optical turbulence is much stronger at low frequencies.[11]

Understanding the vibrations that affect the AAT provides a valuable baseline to determine the effect of future instruments or top-end structural changes. A histogram of the vibration frequencies during our dome turbulence study is shown in Fig. 5. The main vibration occurs at 6 Hz with its harmonic at 12 Hz. The atmospheric dispersion corrector (ADC) was initially considered as the source of the vibration peaks; however, the AAT's ADC update rate is ~0.03 Hz, so it can be excluded as the source. Because the AAT was designed and built to minimize vibration and wind buffeting, the 6-Hz vibration may be the natural frequency of the telescope. The broad frequencies observed between 1 and 13 Hz are likely caused by the flexure within the DOTS instrument and vibration and are not indicative of any telescope vibrations. Unfortunately, the pixel scale (2 arcsec) of the camera limits our ability to analyze the amplitude of the vibrations with most of the motion being under 1.6 $\text{arcsec}^2\,\text{Hz}^{-1}$. The vibration results showed no relationship to any of the meteorological variables tested and showed no trends over time. The significant vibration detection limits of DOTS need to be addressed for future use of the instrument.

2.3 Meteorology

Multiple meteorology variables were recorded in parallel to our dome-seeing-proxy measurements to characterize the seeing conditions in the dome. Some meteorology sensors are located on a water tower dubbed the "golf ball." The golf ball water tower is ~64 m northwest of the AAT. The night assistant sets the air-conditioning in the dome at the end of each night shift for the following night. The forecast minimum temperature and the maximum dew point are used to calculate the set point for the air-conditioning for the next night. During the day, two large fans circulate the air inside the dome and are turned off while the dome is open. Cross-flow fans are located in the primary mirror cell to force mixing.

The meteorology variables recorded are summarized in Table 1. They include multiple temperature sensors, wind speed and direction, humidity, dew point, and barometric pressure. The meteorology variables are acquired every 5 min when DOTS is operational. There is no data available for the pointing of the telescope. Instead, the dome elevation and azimuth were used as the dome points in the same direction as the telescope.

The graph of a meteorology variable versus the dome-seeing-proxy produces a data cloud instead of a well-defined relationship. For this study, we have discretized the meteorology variable values into equally spaced bins and taken the median dome-seeing-proxy value for each bin. These are displayed as a scatter plot instead of a bar graph for clarity. If the average of a variable is taken instead of the median, it is explicitly stated with the graph. Bins with less than 50 data points have a high degree of variability and were not used in the trend line fitting (these data points were given red markers on their respective graphs).

Table 1 Descriptions for the sensor and location of each meteorology variable.

Meteorology variable	Recording instrument	Comments
Outdoor temperature	MetPak Pro weather station	Near boom gate, ~100 m north of the AAT. This weather station is relatively close to the ground (height of 2 m), especially with respect to the AAT primary mirror, which is about 30 m above ground level
Indoor temperature	MetPak Pro weather station	South walkway inside the dome
Mirror temperature	MetPak Pro weather station	Measures the air temperature a few millimetres above the mirror[18]
Wind speed and direction	Ultrasonic method	Located on the top of the golf ball, the data are therefore influenced by the AAT structure to the southeast[18]
Dome elevation and azimuth	Portable telescope control system	Since no data are available for the pointing of the telescope itself, the dome elevation and azimuth is a good proxy as they point in the same direction
Humidity	MetPak Pro weather station	Near boom gate, ~100 m north of the AAT, and another sensor on the south walkway
Sky-ambient temperature	Boltwood cloud sensor	Roof of mechanical building, ~60 m northeast of the AAT
Dew point (outside)	MetPak Pro weather station	Near boom gate, ~100 m north of the AAT
Dew point (inside)	MetPak Pro weather station	South walkway inside the dome
Barometric pressure	MetPak Pro weather station	Near boom gate, ~100 m north of the AAT

3 Turbulence Results

Before going into deeper analysis, an appreciation of the overall turbulence trends at the AAT is useful. A histogram of the dome-seeing-proxy values over the whole time range is shown in Fig. 6(a). The log-normal distribution has a median of 0.29 arcsec, the mode is 0.11 arcsec, and the mean is 0.38 arcsec. The cumulative distribution function [Fig. 6(b)] shows 90% of the dome-seeing-proxy values below 0.75 arcsec. The 10'th, 25'th, 50'th (median), 75'th, and 90'th percentiles are shown in Table 2 for the complete data range and each season. The 10'th and 25'th percentiles are very similar for each season. Spring and autumn have very similar medians; winter has a slightly better median, whereas summer has a slightly worse median. This trend continued for the 75'th and 90'th percentiles.
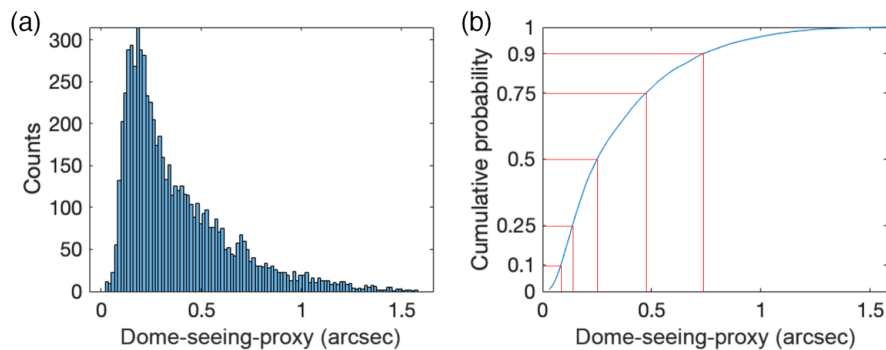

Fig. 6 (a) Histogram of dome-seeing-proxy values; the median dome-seeing-proxy is 0.29 arcsec. (b) The cumulative distribution function for the dome-seeing-proxy values; 90% of the data is <0.75 arcsec.

Table 2 Seasonal trends for the 10'th, 25'th, median, 75'th, and 90'th percentile of dome-seeing-proxy.

	Dome-seeing-proxy percentiles (arcsec)				
	10'th	25'th	Median	75'th	90'th
Autumn	0.13	0.19	0.29	0.50	0.73
Winter	0.12	0.17	0.25	0.46	0.69
Spring	0.13	0.19	0.30	0.49	0.71
Summer	0.12	0.20	0.34	0.61	0.84
All data	0.13	0.18	0.29	0.51	0.75

3.1 Temperature Gradients

Temperature gradients and wind speed have the greatest effect on the dome-seeing-proxy of all the tested meteorology variables. Temperature gradients (ΔT) are one of the most significant contributors to atmospheric turbulence. Air's refractive index is temperature dependent, and pockets of air with inhomogeneous refractive index create a dynamically changing optical path length difference across a pupil as the different temperatures mix. The mixing can either be controlled by the temperature gradient itself or be actively mixed by the wind. Because turbulence is a form of energy dissipation, turbulence will exist in a system where different temperatures are allowed to mix, and a minimum in turbulence will occur at $\Delta T = 0$. Temperature gradients are also a major contributor to dome turbulence; Fig. 7 shows the graphs of the median dome-seeing-proxy versus outdoor-indoor ΔT (a) and median dome-seeing-proxy versus indoor-mirror ΔT (b).

Although the coefficient of determination is high for both these graphs (expressing the goodness of fit of the parabolas), it can be seen that the negative values are rising more steeply than the positive values. In the publication for the initial results for DOTS[19] and other publications,[8] the minimum for the parabola is translated by ~1°C, with the deviation from the theoretical minimum at $\Delta T = 0$ being attributed to a possible temperature sensor offset. The temperature offset between the AAT indoor and outdoor sensors was found to be 0.2°C. The mirror temperature sensor is only accessible during the mirror's extraction for aluminizing. However, temperature readings close to the mirror temperature sensor had an offset of 0.9°C. The minimum value for the parabolas fitted to the temperature gradient graphs is very close to zero once the offset has been considered. Even with the offset explained, the parabolas appear to be non-symmetrical. This is also noted by Salmon et al.,[8] where the two sides of the curve are fitted separately. It can
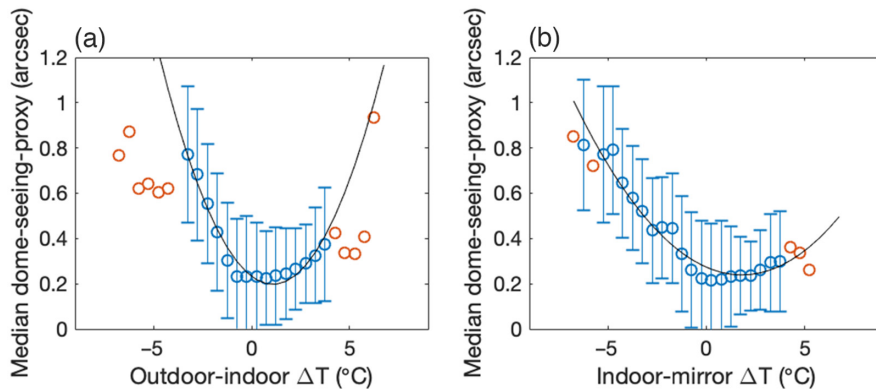

Fig. 7 (a) Outdoor-indoor ΔT versus median dome-seeing-proxy for each 1/2°C temperature difference. (b) Indoor-mirror ΔT versus median dome-seeing-proxy for each 1/2°C temperature difference. Error bars represent one standard deviation.

be shown with the data collected by DOTS that there are conditions (such as wind speed) that only affect the dome-seeing-proxy during convective conditions, pointing to a possible contributor to the non-symmetric temperature gradient curves.

3.2 *Convection Versus Thermal Inversion*

There is a large difference in the dome-seeing-proxy statistics for convection and thermal inversion conditions. In terms of dome turbulence, convection occurs freely when the warmer body is closer to the ground and allows heat to flow upwards. Conversely, thermal inversion is when the warmer body is above the colder body, and convective temperature mixing is suppressed. For this study, convection is defined as the primary mirror being warmer than the surrounding dome air, and the dome air is warmer than the outside air. Conversely, for this study, thermal inversion is defined as when the primary mirror is colder than the surrounding dome air, and the dome air is colder than the outside temperature. Figure 8(a) shows the histograms of convection ($T_{\text{Mirror}} > T_{\text{Indoor}} > T_{\text{Outdoor}}$), and Fig. 8(b) shows thermal inversion ($T_{\text{Mirror}} < T_{\text{Indoor}} < T_{\text{Outdoor}}$) on the right. Convection accounts for 44% of the data, and thermal inversion accounts for 29% of the data. The median for convection is 0.43 arcsec, and the median for thermal inversion is 0.25 arcsec. This is not due to convection having worse temperature statistics, as absolute values for the temperature statistics are very similar for the two datasets.

There are two mixed states of convection and inversion: mirror convection/dome inversion is when the mirror is warmer than the inside air, and the inside air is colder than the outside air ($T_{\text{Mirror}} > T_{\text{Indoor}}$ and $T_{\text{Indoor}} < T_{\text{Outdoor}}$). Mirror inversion/dome convection is when the mirror is colder than the inside air, and the inside air is warmer than the outside air ($T_{\text{Mirror}} < T_{\text{Indoor}}$ and $T_{\text{Indoor}} > T_{\text{Outdoor}}$). The percentiles for convection, inversion, mirror convection/dome inversion, and mirror inversion/dome convection are shown in Table 3.

The mirror inversion/dome convection dataset appears to have excellent seeing statistics according to Table 3. However, this is due to it having a very high percentage ($\sim$90%) of its data very close to zero temperature difference rather than an indication of how the mirror inversion/dome convection state influences the dome-seeing turbulence. No conclusive statements can be made about how these mixed states influence the turbulence due to the small number of data points for these categories. A reason why convection conditions cause worse seeing than thermal inversion conditions has been previously stated, the eddies resulting from convection are far more vigorous and unstable than those resulting from thermal inversion. With the boundary between the temperatures being more unstable in convection, the wind speed can have a more significant degrading effect on the dome-seeing-proxy.

Figure 9(a) shows that the relationship between wind speed and dome-seeing-proxy is linear for convection, with a coefficient of determination of 0.7.

The gradient of the linear relationship is 0.0125 $\frac{\text{arcsec}}{\text{km h}^{-1}}$. Median dome-seeing-proxy versus wind speed has a very low coefficient of determination (0.07) for thermal inversion conditions, showing the fitted line has a similar goodness of fit to a line with zero gradient. This indicates no
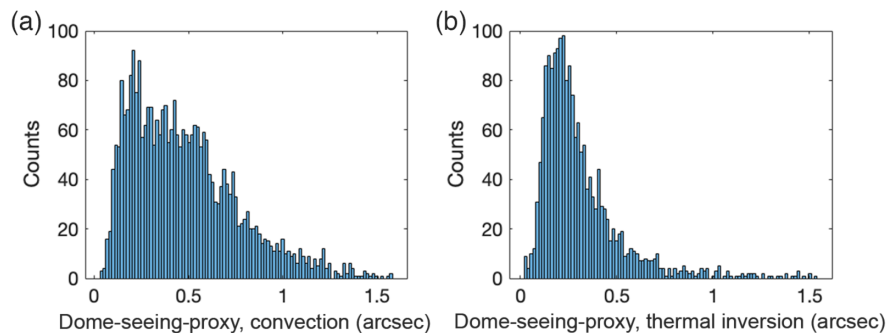

Fig. 8 (a) Histogram of dome-seeing-proxy for convection data only. (b) Histogram of dome-seeing-proxy for thermal inversion data only. The log-normal distribution is much more skewed for the convective case than the thermal inversion case. The median dome-seeing-proxy is 0.43 arcsec for convection and 0.25 arcsec for thermal inversion.

Table 3 Seasonal trends for the 10'th, 25'th, median, 75'th, and 90'th percentile of dome-seeing-proxy.

	Dome-seeing-proxy percentiles (arcsec)				
	10'th	25'th	Median	75'th	90'th
Convection (44%)	0.16	0.25	0.43	0.64	0.87
Thermal inversion (27%)	0.13	0.18	0.25	0.38	0.56
Mirror convection/dome inversion (10%)	0.13	0.17	0.24	0.41	0.65
Mirror inversion/dome convection (15%)	0.10	0.13	0.19	0.32	0.57
All data	0.13	0.19	0.29	0.51	0.75
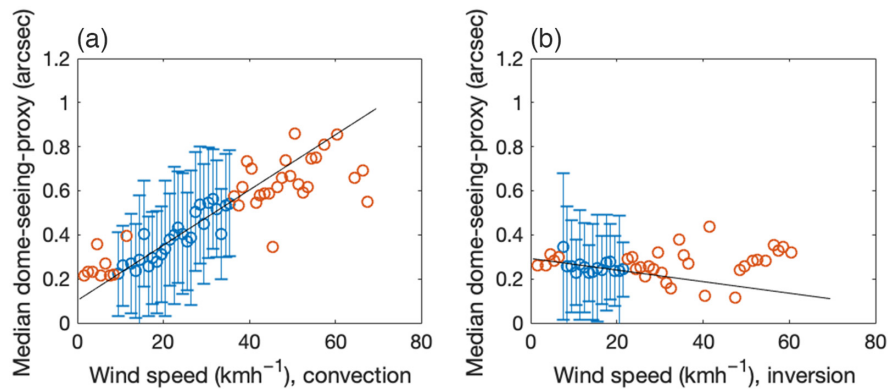
Fig. 9 (a) Median dome-seeing-proxy versus wind speed for convection conditions. (b) Median dome-seeing-proxy versus wind speed for thermal inversion conditions. Error bars represent one standard deviation.

discernible relationship between the wind speed and the dome-seeing-proxy for thermal inversion conditions. This is due to higher wind speeds being correlated with lower outside temperatures, which drives the conditions toward convection. Therefore, it is difficult to disentangle the effect of wind speed from the temperature gradient for convection conditions. To try and disentangle the two factors, Fig. 10 shows the median dome-seeing-proxy versus the outdoor-indoor ΔT, separated into three different wind speed brackets: 0 to 15 kmh^{-1}, 15 to 30 kmh^{-1}, and 30 to 45 kmh^{-1}. The error bars are left off this graph for clarity, but the standard deviations for each data point are similar. It can be seen that the 0 to 15 kmh^{-1} winds have little effect on the skewness of the parabola. The 15 to 30 kmh^{-1} wind speeds increase the convection values (negative values of ΔT) while not influencing the inversion values (positive values of ΔT). The effect is even more substantial for the 30 to 45 kmh^{-1} bracket, but there is no inversion data for comparison in this wind speed bracket.

Furthermore, the 30 to 45 kmh^{-1} gradient is similar to the other wind speed categories. This supports the conclusion that wind speed independently influences dome-seeing-proxy from the temperature gradient. This result can be used to contribute to the explanation of why convection conditions result in worse dome-seeing-proxy medians.

The residual shift in minimums seen in the median dome-seeing-proxy versus ΔT graphs even after the sensor offsets have been accounted for (Fig. 7) is likely due to fitting algorithms accounting for the steeper rise in negative ΔTs than for positive ΔTs. The "skewness" imparted by the wind speed and convection eddies preserves the theoretical minimum value at $\Delta T = 0$.

From this data, lowering the set point temperature for the air-conditioning to bias the temperatures toward inversion would be worth considering. Although this would be ideal in theory, a
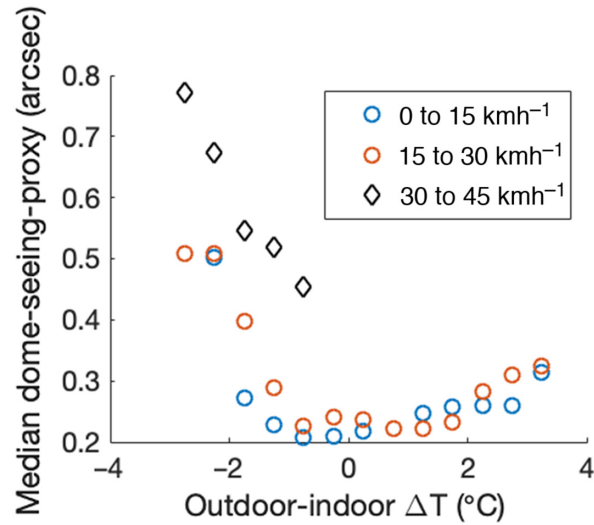
Fig. 10 Median dome-seeing-proxy versus outdoor-indoor ΔT for low wind speed (blue circles), medium wind speed (red circles), and high wind speed (black diamonds).

few operational constraints limit the feasibility- one of the major constraints concerns relative humidity.

The relative humidity is a particular concern at the AAT; it has a much higher level of humidity than other scientific telescopes, with an average of about 60.3%.[20] The AAT has limited capacity to clean the primary mirror *in situ*, which makes condensation on the primary mirror a highly undesirable event. Consequently, careful attention is given to the inside and outside dew points. If the dome interior is cold and a warm front comes over the site, it greatly increases the risk of condensation. The difference in relative humidity between the outdoor and indoor sensors is highly correlated to the outdoor-indoor ΔT and also has a parabolic relationship to the dome-seeing-proxy, as shown in Fig. 11.

3.3 Elevation

The general results for the dome elevation (and therefore the telescope elevation) show little effect on the dome-seeing-proxy. However, there is a notable difference when the dataset is again
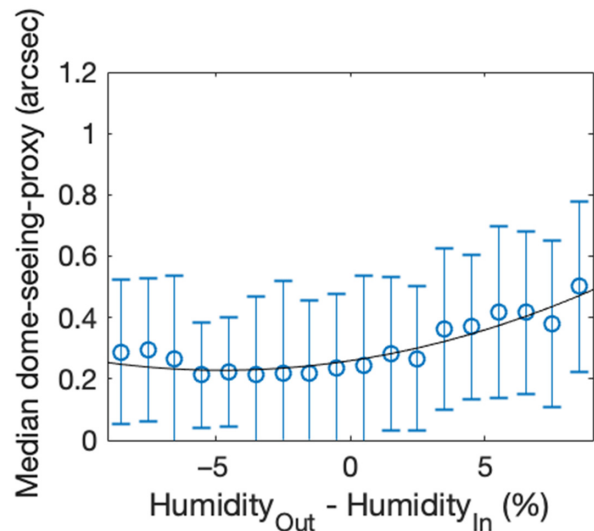

Fig. 11 Median dome-seeing-proxy versus difference between outdoor and indoor relative humidity. Error bars represent one standard deviation.
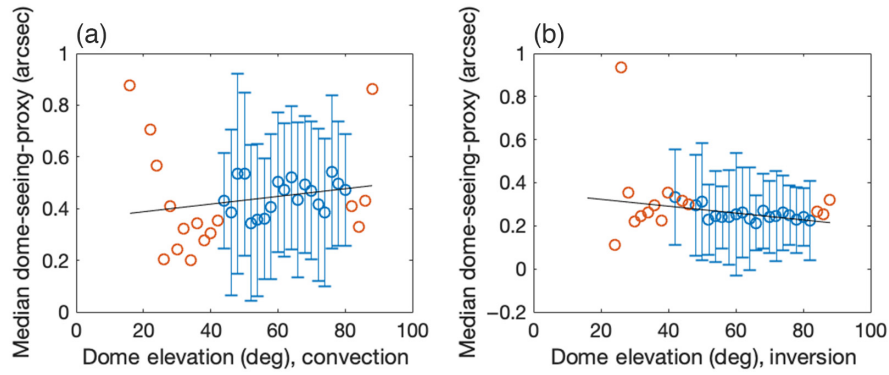
Fig. 12 (a) Median dome-seeing-proxy versus dome elevation for convection conditions. (b) Median dome-seeing-proxy versus dome elevation for thermal inversion conditions. Error bars represent one standard deviation.

divided into convection and inversion. Figure 12(a) shows the relationship between dome elevation and dome-seeing-proxy for the convection case, and [Fig. 12(b)] the relationship between dome elevation and dome-seeing-proxy for the thermal inversion case. Since warm air rising from the primary mirror influences more of the optical path the closer the telescope is to zenith, the convective case is expected to produce a relationship between elevation and dome seeing. The convection graph has a very poor coefficient of determination (0.01), indicating the fit is no better than a line with zero gradient. Even though there is a visual difference between the convection and inversion case for dome elevation, no conclusions about the effect of elevation can be drawn here. This is dissimilar to many other telescopes that exhibit a relation between elevation and dome turbulence strength; for example, the CFHT shows an increase in seeing above 65 deg elevation.[8]

3.4 Relative Wind Direction

Interestingly, unlike the dome seeing at CFHT,[8] the relative wind direction to the dome slit has little effect on the dome-seeing-proxy at the AAT. For Fig. 13, we introduce θ as the angle between the wind direction and the dome slit pointing; at $\theta = 0$, the dome slit is pointing into the wind, and at $\theta = 180$, the dome slit is pointing directly away from the wind. There is a weakly correlated linear relationship with a shallow negative gradient, showing that the seeing
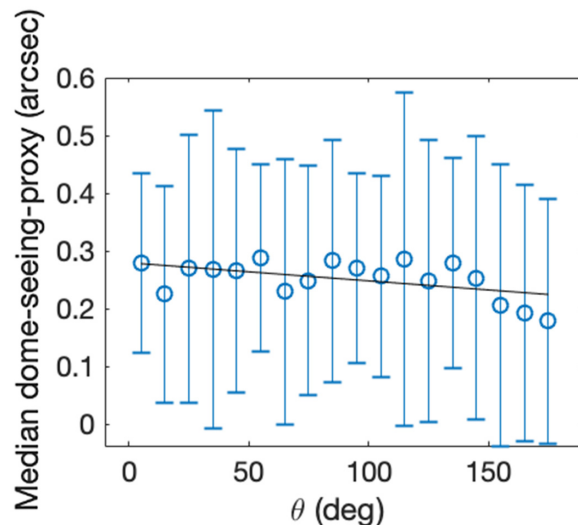

Fig. 13 Median dome-seeing-proxy versus relative wind direction (θ). Error bars represent one standard deviation.
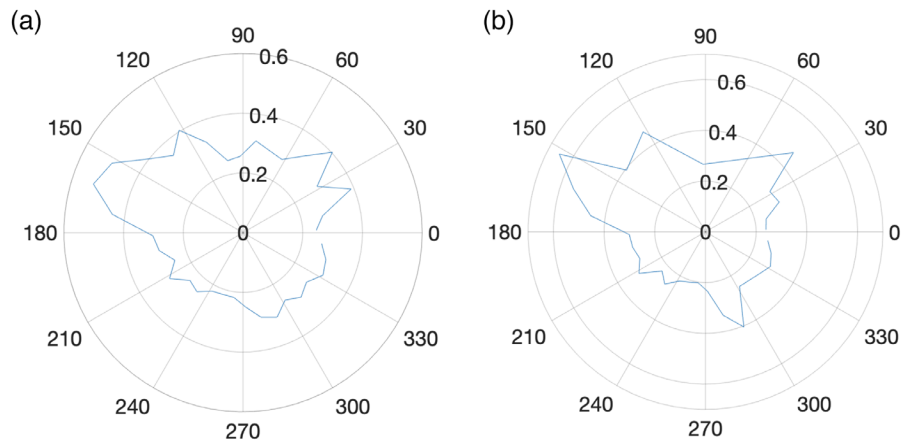
Fig. 14 Median dome-seeing-proxy versus dome azimuth. Median dome-seeing-proxy (arcsec) is presented as the radial value, and the telescope azimuth is represented by the angle in degrees. The error bars are not included for clarity, but the values all have similar standard deviations. (a) all elevation values and (b) 0 deg to 70 deg elevation values.

conditions in the dome are slightly better when the dome slit is pointing directly away from the wind. This result is largely independent of wind speed, but this cannot be definitively confirmed in this study, as dividing the dataset by relative wind direction and then also sorting into wind brackets (as used for Fig. 10) leaves the counts too low in each category for robust comparison. Since the θ of the wind has a limited effect on the dome-seeing-proxy values inside the dome, it is likely that the eddies that contribute to the mixing of temperatures at the dome boundary do not contribute significantly to air movement near the optical path of the telescope. This may be a consequence of the very large dome size of the AAT compared to similar sized telescopes.

3.5 *Azimuth*

Figure 14(a) shows the rose plot of the azimuth angle (with respect to north) against the median dome-seeing-proxy with all data, and only elevation angles below 70 deg [Fig. 14(b)]. Above elevation angles of 70 deg, there is no discernible relationship between azimuth angle and dome-seeing-proxy. There is a substantial peak (approximately twice the background) at Az 165 deg, seen in the full dataset [Fig. 14(a)], and even more prominently in the elevations lower than 70 deg dataset [Fig. 14(b)]. This peak is independent of relative wind direction. One reason for this 165 deg is the bearing on which the air-conditioning vents supplying cold air to the dome are centred. Three factors could contribute to the dome-seeing-proxy being worse at Az 165 deg. First, the area is clear of any other support structures or rooms, giving the area different thermal inertia from other parts. Second, it is inevitably slightly colder than other places in the dome, exacerbating any temperature gradients. Third, the air-conditioning forces air around, creating mechanical turbulence not seen elsewhere in the dome. Two smaller peaks can be seen at Az 42 deg and Az 292 deg, which become much more evident under 70 deg dome elevation [Fig. 14(b)]. These peaks correspond to the air-conditioning return vents located at these bearings from the telescope. Since these vents are sucking in air and not contributing to any temperature gradient, the peak in dome-seeing-proxy is likely due to mechanical turbulence.

4 Seasonal Trends

La Nina (increased rain) events were common over the 2021 to 2022 period the DOTS data were collected. Considering these La Nina events followed a short and severe drought, the period 2021 to 2022 does not closely resemble the average weather conditions at SSO. Therefore more data over many more years would be needed before concluding the seasonal trends presented here as universal.

Table 4 Seasonal trends for the 10'th, 25'th, median, 75'th, and 90'th percentile of seeing.

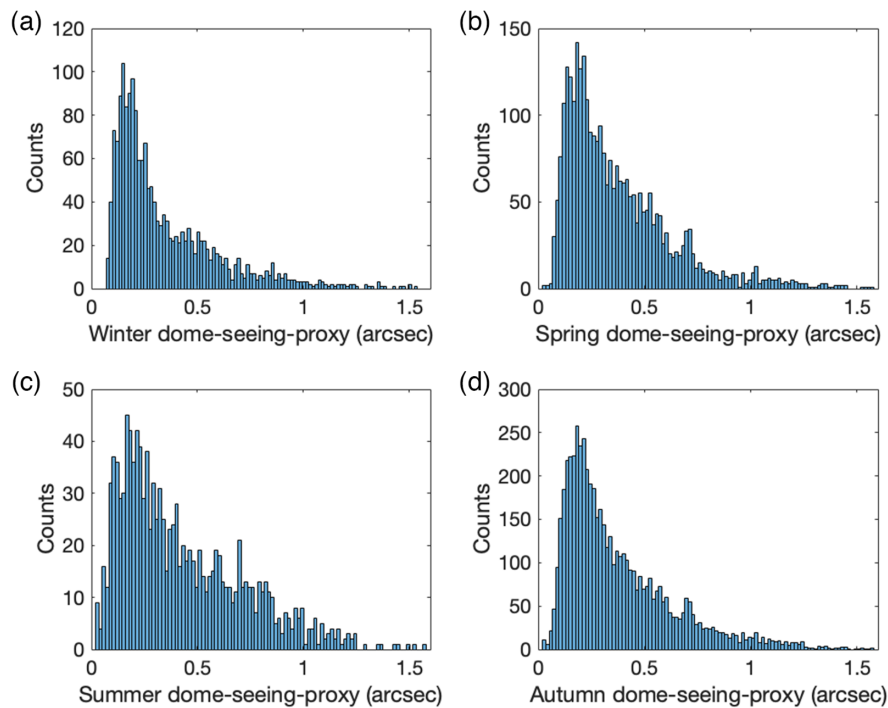|	Dome-seeing-proxy percentiles (arcsec)				
	10'th	25'th	Median	75'th	90'th
Autumn	0.13	0.19	0.29	0.50	0.73
Winter	0.12	0.17	0.25	0.46	0.69
Spring	0.13	0.19	0.30	0.49	0.71
Summer	0.12	0.20	0.34	0.61	0.84
All data	0.13	0.18	0.29	0.51	0.75

Fig. 15 Histograms of the dome-seeing-proxy for (a) winter, (b) spring, (c) summer, and (d) autumn.

The seasonal trends for the dome-seeing-proxy are shown in Table 4. The data are divided into the 10'th, 25'th, median, 75'th, and 90'th percentiles. The data are also visualized using histograms for each season, as shown in Fig. 15. It can be seen that summer has the worst turbulence values with winter having the best turbulence values. The 10'th and 25'th percentiles are very similar for each season. Spring and autumn have very similar medians; winter has a slightly better median, whereas summer has a slightly worse median. This trend continued for the 75'th and 90'th percentiles. For the 75'th and 90'th percentiles, summer has about 0.2 arcsec worse seeing than winter and 0.1 arcsec worse seeing than autumn and spring.

Initially, it was thought that this might be due to the thermal inertia of the telescope and housing having a more significant effect during the warmer months, where the maximum and minimum temperature difference is larger. The difference between the maximum and minimum temperature overnight was tested, and the largest temperature changes were in spring and summer. Using the data published by Abbot et al.,[20] the 24-hr temperatures show that the difference between the maximum and minimum temperature is much greater in summer, nearly

Table 5 Seasonal median dome-seeing-proxy values for convection and inversion.

	Convection		Inversion	
	Median dome-seeing-proxy	% of observations	Median dome-seeing-proxy	% of observations
Autumn	0.45	42%	0.25	32%
Winter	0.33	53%	0.26	12%
Spring	0.47	42%	0.25	39%
Summer	0.51	53%	0.25	22%

identical in autumn and spring and lower in winter. This suggests that the higher thermal heating of the dome structure and building during the day significantly affects the dome-seeing-proxy even though the dome is actively cooled with air-conditioning during the day.

A possible mechanism that explains why the extra heating greatly influences the summer dome-seeing-proxy statistics is that the extra heating causes a higher percentage of the summer data to be in convection. The percentages of observations in convection and inversion for their respective seasons are shown in Table 5.

The higher incidence of convective conditions in summer significantly contributes to the worse seeing conditions, as convective conditions are susceptible to further degradation by wind speed. In contrast, thermal inversion is indifferent to wind speed. Winter also has a higher incidence of convection conditions, but it has much better dome-seeing-proxy statistics than summer; this is partly due to summer having much higher wind speeds than the other seasons and winter having lower wind speeds.

Since we know that both temperature gradients and wind speed affect the dome-seeing-proxy and convection eddies, we can define a range of favorable conditions as the range over which the median dome-seeing-proxy is less than the median for the whole dataset. Table 6 shows the percentage of data for each season that falls in the favorable range for outdoor-indoor ΔT, indoor-mirror ΔT, and wind speed.

Summer has a significantly lower percentage for both favorable temperature gradient ranges. In comparison, winter has a slightly lower percentage for outdoor-indoor ΔT but a similar percentage to autumn and spring for indoor-mirror ΔT. Summer also has a significantly lower percentage of favorable wind speeds, with just 55% compared to 69% for autumn, 73% for spring, and 79% for winter. This is reflected in the histograms of wind speed for the different seasons, as shown in Fig. 16. Winter has an easily recognizable log-normal distribution. Spring and autumn have a less skewed log-normal shape with a higher level of noise. Summer shows a much less skewed log-normal relationship. The degree of symmetry even makes the histogram similar to a Gaussian shape. Due to the different distribution shapes, comparing the medians and even the means of these datasets does not reflect the difference in wind conditions. The difference in distribution is likely to contribute to the worse seeing conditions during summer.

Table 6 Percentage of data for each season that falls within a "favorable" range for temperature gradients and wind speed.

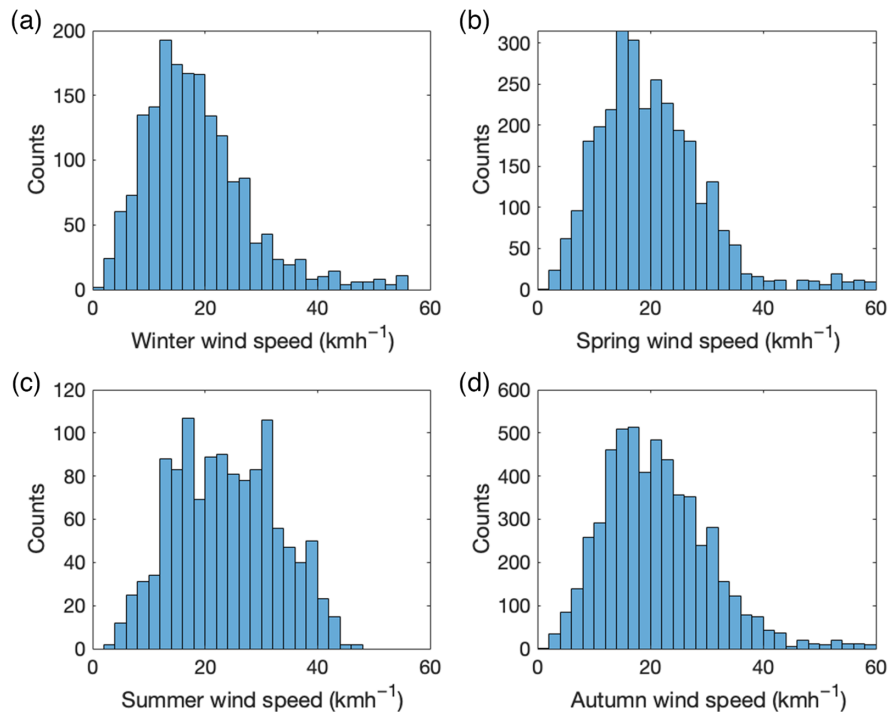|	Percentage of data within the favorable range		
	Outdoor-indoor ΔT	Indoor-mirror ΔT	Wind speed
Autumn	55%	57%	69%
Winter	50%	57%	79%
Spring	55%	62%	73%
Summer	43%	52%	55%

Fig. 16 Histograms of the wind speed for winter (a), spring (b), summer (c), and autumn (d).

5 Hourly Trends

As with the presented seasonal trends, hourly trends should not be considered universal because our study only has 89 nights worth of data spanning over 1 year. The hourly trends are interesting to investigate here as they have previously been studied at the AAT and comparisons with these previous studies can be made.

Ryan and Wood[15] published a 1995 dome seeing study of the AAT that showed that the seeing degrades over the night, with seeing at local times 17 to 22 hrs, 22 to 02 hrs and 02 to 07 hrs being 1.3 arcsec, 1.5 arcsec and 1.6 arcsec, respectively. Their findings support that, first, the time dependence is not a seasonal effect, and second, that the indoor-mirror ΔT is the dominant factor for the time dependence with the outdoor-indoor ΔT having little effect.

We have tested these observations against the observations made with DOTS. It should be noted that the dataset collected by DOTS is much larger than the 1995 study. We found a similar degradation throughout the night with median dome-seeing-proxies of 0.26 arcsec, 0.29 arcsec, and 0.35 arcsec for the three time periods 17 to 22 hrs, 22 to 02 hrs, and 02 to 07 hrs, respectively. The much better medians measured in this study compared to the 1995 study is likely due to the more efficient thermal control of the dome compared to 1995. However, unlike the 1995 study, the DOTS data show a seasonal trend. Figure 17 shows a bar graph of the median dome-seeing-proxy for the three time periods and each season.

Spring and autumn have moderate degrees of degradation throughout the night. Summer experiences the highest degree of degradation, particularly at the end of the night. Winter shows only a small degree of degradation, notably with the middle part of the night being slightly lower than the start. The DOTS dataset, therefore, supports the conclusion that the time dependence of the dome-seeing-proxy is not independent of the seasons. This is most likely a consequence of stronger temperature gradients in the warmer months of the year, as well as higher wind speeds during the warmer months. However, with data only spanning 2021 to 2022, we cannot conclude that this is the universal trend across different seasons. Since SSO can experience substantially different conditions from year-to-year, an extended study would be needed to confirm the trend. Another possible reason for the differing results from the 1995 study is that the temperature controls in the telescope are now very different since the addition of air-conditioning in the mid-2000s.
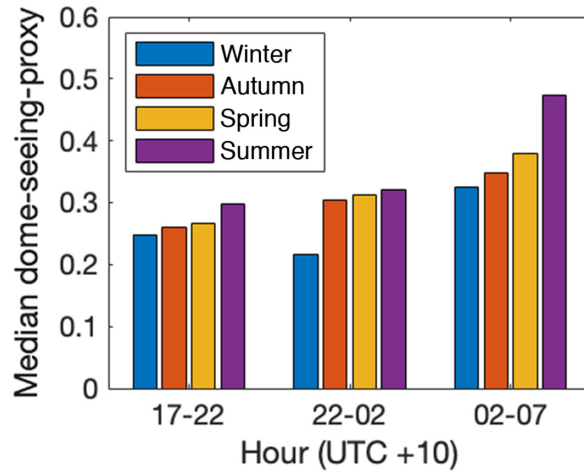
Fig. 17 Bar graph showing the median dome-seeing-proxy for the start (17 to 22 hr), middle (22 to 02 hr), and end (02 to 07 hr) local times of the night, separated into different seasons.
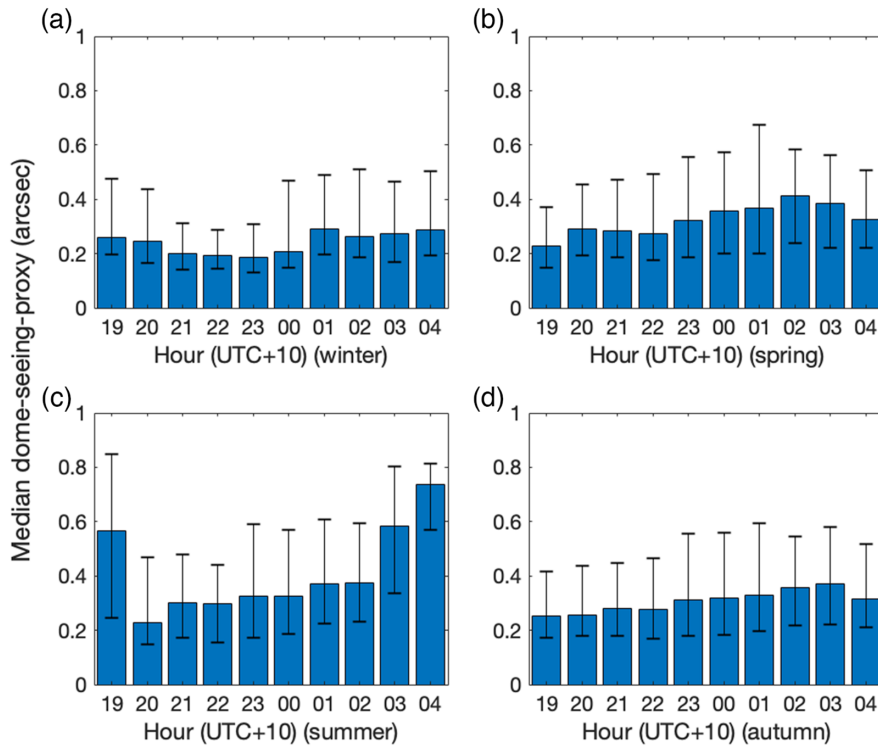

Fig. 18 Bar graph showing the local hourly median dome-seeing-proxy values for winter (a), spring (b), summer (c), and autumn (d). The error bars for these graphs are the 25'th and 75'th percentile instead of the standard deviation used for error bars in previous sections of this paper.

Since thousands of data points are available from DOTS for each season, we can also look into the hourly median dome-seeing-proxy to better understand the nightly degradation trend. Figure 18 shows the hourly median dome-seeing-proxy for each season. The error bars for these graphs are the 25'th and 75'th percentile instead of the standard deviation used for error bars in previous sections of this paper. This highlights the data distribution with skewed ranges indicative of log-normal distributions and even ranges indicative of a Gaussian shape. A Gaussian shape rather than a log-normal shape may indicate that the turbulence is not fully evolved in the dome, but this assumption needs to be tested.

Winter again shows a dip in median dome-seeing-proxy during the middle of the night before rising at the end of the night. Spring and autumn are similar, with the dome-seeing-proxy slowly rising until 02 to 03 hrs, then slightly dipping back down at the end of the night. Summer shows a very different trend, starting with a median dome-seeing-proxy of ~0.8 arcsec at the start of the night, dropping quickly to a minimum of ~0.2 arcsec at 20 hrs and then rising back up to ~0.8 arcsec by the end of the night.

The DOTS dataset is considerably larger than the dataset used by Ryan and Wood,[15] with ~10,000 data points compared to 100. With this, we can present a much more detailed hourly analysis. We present the hourly median temperature gradients, the median wind speed, relative humidity, and the median raw outdoor, indoor, and mirror temperatures for each season. Autumn and spring are grouped together as the conditions and patterns in their results are very similar. Winter is grouped with summer to fully juxtaposed their very different conditions and patterns.

5.1 Autumn and Spring

Autumn [Fig. 19(a)] has a slow degradation of the dome-seeing-proxy until 03 hrs, then a slight improvement at the end of the night. This trend is supported by both temperature gradients show inversion until about 22 hrs [Fig. 19(b)]. The median raw temperatures graph [Fig. 19(c)] show the indoor and mirror temperatures to be colder than the outdoor temperature until about 23 hrs. By about 23 hrs, the indoor temperature is fairly closely following the outdoor temperature, but the mirror temperature is lagging behind substantially. The end of the night sees the temperatures getting closer, minimizing the temperature gradients. The outdoor-indoor ΔT decreases back toward zero in the early hours of the morning while the indoor-mirror ΔT remains firmly in the convection regime. This period of the night corresponds to a decrease
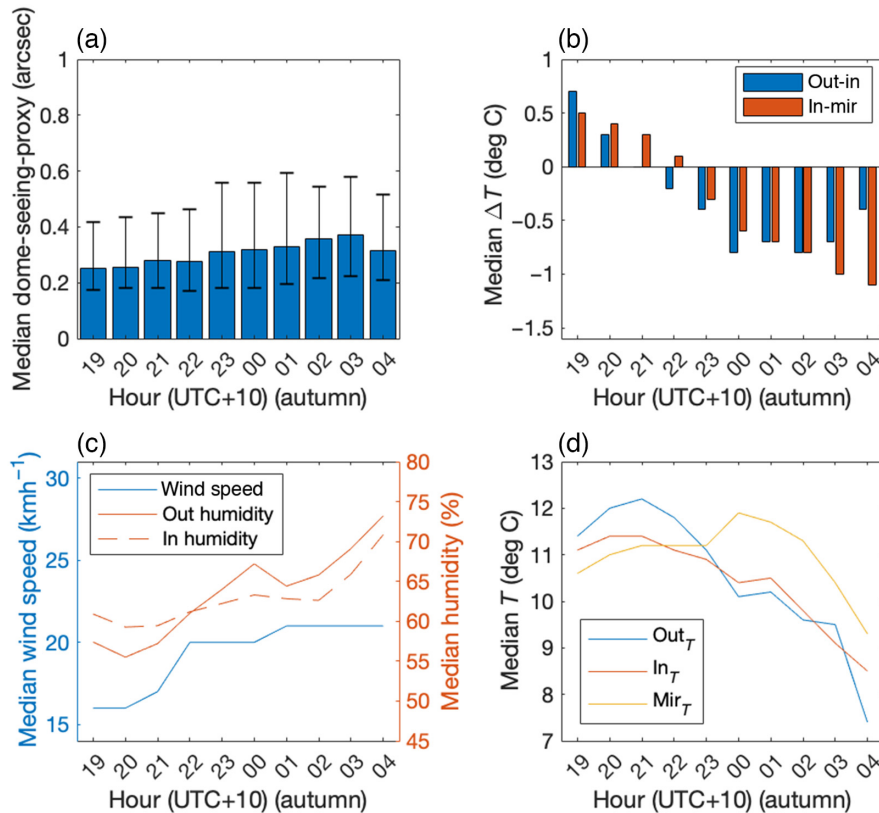

Fig. 19 Autumn medians. (a) Median dome-seeing-proxy throughout the night. The error bars for these graphs are the 25'th and 75'th percentile to highlight any skewed data. (b) Median temperature gradients throughout the night. (c) Median wind speed, outdoor and indoor relative humidity over the course of the night. (d) Median raw temperatures throughout the night.
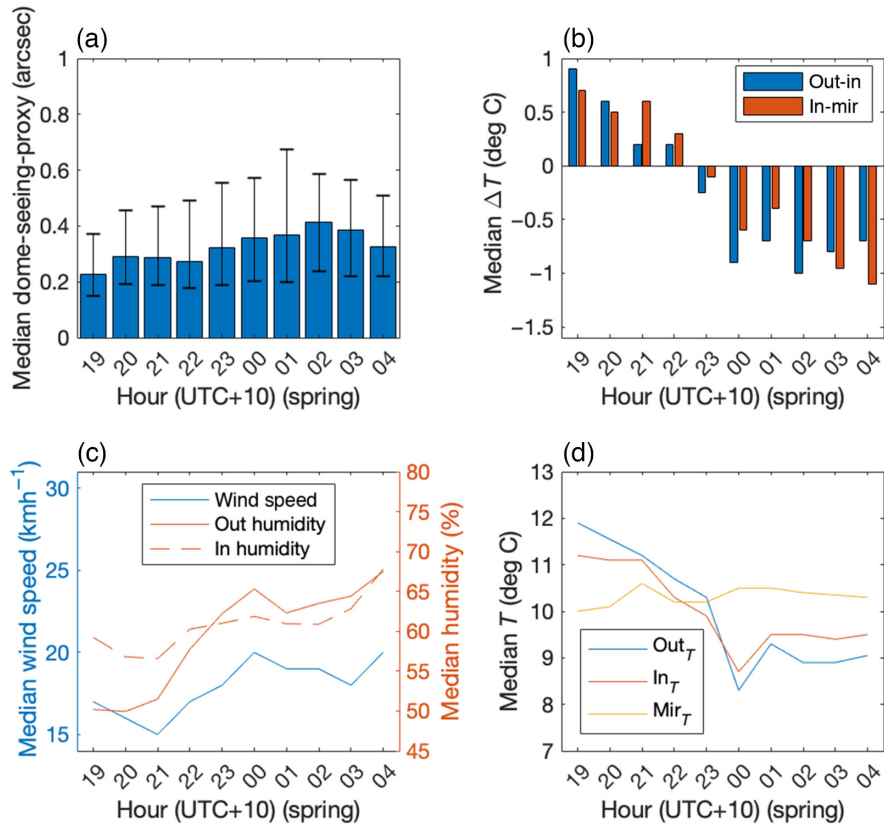
Fig. 20 Spring medians. (a) Median dome-seeing-proxy throughout the night. The error bars for these graphs are the 25'th and 75th percentile to highlight any skewed data. (b) Median temperature gradients throughout the night. (c) median wind speed, outdoor and indoor relative humidity over the course of the night. (d) Median raw temperatures throughout the night.

in the dome-seeing-proxy, suggesting the domes-seeing-proxy has a stronger relationship to the outdoor-indoor ΔT compared to the indoor-mirror ΔT.

Spring (Fig. 20) has a very similar pattern across the night to autumn. The temperatures start the night in inversion conditions, and then at about 23 hrs, the mirror temperature remains stable while the indoor temperature sits slightly above the outdoor temperature.

Since both of the temperature gradients are in good agreement for autumn and spring, it is not possible to disentangle whether the outdoor-indoor ΔT or the indoor-mirror ΔT is the dominant temperature gradient for these seasons, although the outdoor-indoor ΔT appears to have a stronger effect in the early hours of the morning when temperatures are in convection.

5.2 Winter and Summer

Summer (Fig. 21) conditions are quite different to autumn and spring. The wind speed ramps up significantly throughout the night, as does the dome-seeing-proxy. Not shown on the graph is the median wind speed value for 18 hrs, which is ~28 kmh^{-1}, contributing to the higher dome-seeing-proxy seen a the start of the night for summer. We can also see that the summer correlates more to the outdoor-indoor ΔT, especially toward the end of the night. This agrees with the observation that high wind speeds significantly impact the dome-seeing-proxy. The lag in the mirror temperature is most evident in summer and spring, as the temperature difference between the maximum and minimum outdoor temperature is about 4°C in both summer and spring. In autumn and spring, the indoor temperature is seen to follow the outdoor temperature much more closely than in summer, where even by the end of the night, the indoor temperature has not equalized with the outdoor temperature. This is indicative of the extra heating experienced
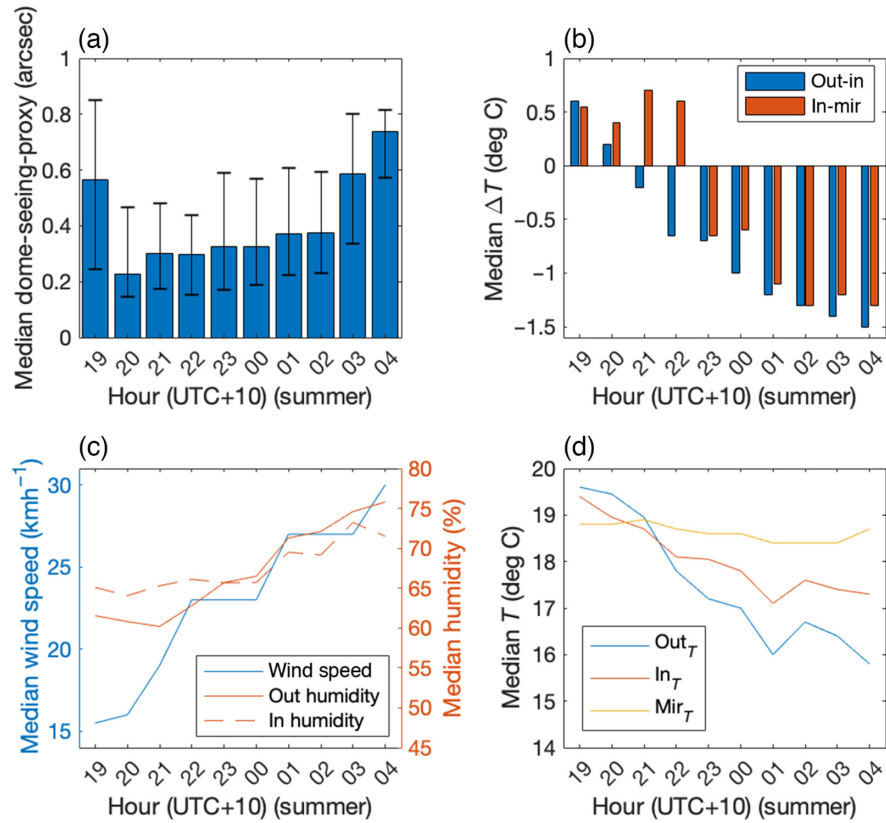
Fig. 21 Summer medians. (a) Median dome-seeing-proxy throughout the night. The error bars for these graphs are the 25'th and 75'th percentile to highlight any skewed data. (b) Median temperature gradients throughout the night. (c) Median wind speed, outdoor and indoor relative humidity over the course of the night. (d) Median raw temperatures throughout the night.

by the whole building during the day in summer, leading to excess heat leaking into the dome from other parts of the building.

Winter also has a very different set of conditions, with much smaller temperature variations and slower wind speeds. This matches our understanding that even though winter has a higher percentage of convection than autumn and spring, it has better dome-seeing-proxy medians. Winter (Fig. 22), conversely to summer, shows a better correlation with the Indoor-Mirror ΔT than the Outdoor-Indoor ΔT. Although the mirror temperature is only a few degrees warmer than the outdoor temperature, it is very rarely colder than the outside temperature.

This result dispels the second point raised in the 1995 study[15] that the indoor-mirror ΔT is the dominant factor for the time dependence with the outdoor-indoor ΔT having little effect. Which temperature gradient is the dominant influence on the dome-seeing-proxy relies on other factors, for example, whether there is convection or inversion and whether the wind speed is high or low. It is likely that they both independently influence the dome seeing but can have either a dominant or muted effect under certain conditions.

6 Discussion and Future Work

One area of improvement for DOTS is relatively simple; the improvement of the optical design to be diffraction limited so that the SNR ratio of the focal spot is maximized. This will lower the amplitude threshold that DOTS can detect, making the instrument more sensitive to vibration. An improvement to the instrument that would increase the accuracy and reliability of the separation between turbulence and vibration data would be to use a DIMM aperture mask. The differential image motion would provide the seeing measurement independently of vibrations, and the vibrations can be simultaneously calculated using the absolute image motion of one of
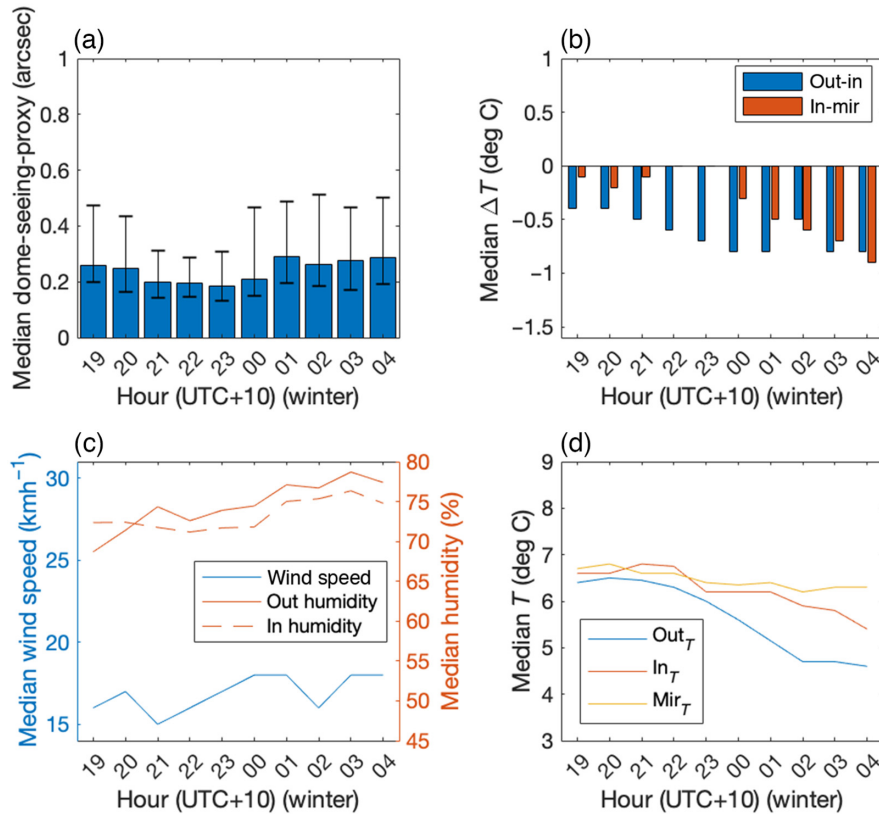
Fig. 22 Winter medians. (a) Median dome-seeing-proxy throughout the night. The error bars for these graphs are the 25'th and 75'th percentile to highlight any skewed data. (b) Median temperature gradients throughout the night. (c) Median wind speed, outdoor and indoor relative humidity over the course of the night. (d) Median raw temperatures throughout the night.

the focal spots. This would also provide a direct quantitative comparison of the DIMM seeing to the derived dome-seeing-proxy. This would determine if the absolute image motion monitor software can be used viably on its own or if the vibration residuals that are unidentifiable through the noise induced by turbulence cause a non-negligible amount of bias.

The applicability of this study would be improved by directly comparing the seeing as measured through the telescope to the dome-seeing-proxy. Unfortunately, the seeing recorded by the AAT is not ideally measured; it is recorded by the night observer at uneven intervals, often after significant weather changes, and is sometimes estimated rather than measured. Each night observer will also likely bias the recording by rounding or estimating differently. These recording errors in the AAT's seeing measurement have been disclosed and discussed in previous AAT dome seeing studies.[15]

7 Conclusions and Recommendations

Since the dome-seeing-proxy is proportional to the actual dome seeing, the relationship trends between the dome-seeing-proxy and the meteorological variables are more reliable than the absolute value of the dome-seeing-proxy. The multiplicative factor between the dome-seeing-proxy and the actual dome seeing can be assumed to be small as SSO has a reported median seeing value of 1.2 arcsec and the AAT has a reported median seeing value of 1.5 arcsec. This agrees well with our median dome-seeing-proxy value of 0.29 arcsec (see Sec. 3). Below is a summary of the most significant results from the DOTS dataset.

- The wind speed only contributes to the dome-seeing-proxy in convection conditions. Its influence is independent of the temperature gradients (see Sec. 3.2)

- The relative wind direction does not significantly impact the AAT dome-seeing-proxy; the dome is so large that the incoming wind has enough space to become unidirectional by the time it reaches the telescope (see Sec. 3.5)
- There are three peaks in the dome-seeing-proxy when plotting against azimuth, which correspond to the air-conditioning vents (see Sec. 3.5)
- Seasonal trends exist, but since we have only 1 year of data, we cannot be sure if they are universal trends or specific to the year past. Summer has the worse median dome-seeing-proxy value (0.34 arcsec), followed by spring (0.30 arcsec) and autumn (0.29 arcsec), and winter has the best median dome-seeing-proxy value (0.25 arcsec) (see Sec. 4)
- Hourly trends also exist for each season (with the same caveat that we cannot confirm if it is a universal trend at the AAT). The trends in each season broadly follow the changes in temperature gradients, combined with knowledge of wind speeds (see Sec. 5)
- Both the outdoor-indoor ΔT and the indoor-mirror ΔT influence the dome-seeing-proxy independently. It can be seen that the outdoor-indoor ΔT becomes more dominant when there is high wind in convection conditions (see Sec. 5.2)

Concerning telescope operations, some recommendations that can be supported by this study include vent deflectors for the air-conditioning ports to improve the azimuth dependence. It would also be worth considering lowering the set point temperature for the air-conditioning to try and include a higher proportion of observations under thermal inversion instead of convection. However, this must be carefully weighed with the risk of condensation in the dome, a major concern for a site with frequently high relative humidity.

With this study, the nature of the AAT's dome turbulence is now known in much more detail. The conditions that influence dome-seeing-proxy have been explored and there is considerable interaction between meteorology variables. The dominant effects are temperature gradients and wind speed. Convection conditions are considerably more detrimental to the dome-seeing-proxy. Furthermore, wind speed is only influential under convection conditions. There are a few minor contributors to the dome-seeing-proxy, such as the air-conditioning vents that cause moderate dome-seeing-proxy to increase at azimuth angles where they are located. Elevation has a complex influence on the dome-seeing-proxy, depending on convection and low wind speed. However, the complete set of conditions necessary for the elevation to influence the dome-seeing-proxy could not be identified in this study. Unlike other large telescopes, the very large dome size of the AAT results in no discernible relationship between the relative wind direction and the dome-seeing-proxy. Future studies of dome seeing and vibrations would be of significant value as a much more robust baseline for data comparison now exists.

Acknowledgments

Code, Data, and Materials Availability

Data are available from the corresponding author upon reasonable request.

References

1. C. R. Masson, "Seeing," *Symp. – Int. Astron. Union* **158**, 1–10 (1994).
2. P.-Y. Bely, "Weather and seeing on Mauna Kea," *Publ. Astron. Soc. Pac.* **99**, 560 (1987).

3. A. A. Radu et al., "An astroclimatological study of candidate sites to host an imaging atmospheric Cherenkov Telescope in Romania," *Mon. Not. R. Astron. Soc.* **422**, 2262–2273 (2011).

4. G. Lombardi, V. Zitelli, and S. Ortolani, "The astroclimatological comparison of the Paranal Observatory and El Roque de Los Muchachos Observatory," *Mon. Not. R. Astron. Soc.* **399**, 783–793 (2009).

5. W. Skidmore et al., "Thirty meter telescope site testing V: seeing and isoplanatic angle," *Publ. Astron. Soc. Pac.* **121**(884), 1151–1166 (2009).

6. D. Macmartin et al., "Primary mirror dynamic disturbance models for TMT: vibration and wind," *Proc. SPIE* **7738**, 77380E (2010).

7. N. Woolf, "Dome seeing," *Publ. Astron. Soc. Pac.* **91**, 523 (1979).

8. D. Salmon et al., "CFHT image quality and the observing environment," *Publ. Astron. Soc. Pac.* **121**(882), 905–921 (2009).

9. M. Baril et al., "An aerodynamic study of the CFHT dome using water tunnel tests and CFD," *Proc. SPIE* **8449**, 844903 (2012).

10. O. Lai et al., "Direct measure of dome seeing with a localized optical turbulence sensor," *Mon. Not. R. Astron. Soc.* **484**, 5568–5577 (2019).

11. E. Bustos and A. Tokovinin, "Dome seeing monitor and its results for the 4m Blanco Telescope," *Proc. SPIE* **10700**, 107000Q (2018).

12. M. Goodwin, C. Jenkins, and A. Lambert, "Characterisation of the optical turbulence at siding spring," *Publ. Astron. Soc. Aust.* **30**, e009 (2013).

13. M. Goodwin et al., "Adaptive optics on-sky demonstrator for the Anglo-Australian Telescope," *Proc. SPIE* **9909**, 990933 (2016).

14. P. R. Gillingham, "Seeing measurements at the Anglo-Australian Telescope," *Proc. SPIE* **0444**, 165–174 (1983).

15. S. G. Ryan and P. R. Wood, "Seeing degradation within the Anglo-Australian Telescope dome," *Publ. Astron. Soc. Aust.* **12**(1), 89–94 (1995).

16. A. R. Sengupta and R. Jensen-Clem, "Kalman filtering for tip-tilt correction in adaptive optics," *Res. Notes AAS* **4**, 244 (2020).

17. B. L. Roux et al., "Kalman-filter-based optimal control law for star-oriented and layer-oriented multiconjugate adaptive optics," *Proc. SPIE* **5490**, 1336–1346 (2004).

18. J. Cameron, "AAT weather data," Australian National University, 2022, http://aat-ops.anu.edu.au/AATdatabase/met.html (accessed 16 March 2022).

19. J. Munro et al., "Results of the dome turbulence sensor at the Anglo-Australian Telescope," *Proc. SPIE* **12186**, 121860A (2022).

20. H. J. Abbot et al., "Archival weather conditions at siding spring observatory," *Publ. Astron. Soc. Pac.* **133**, 095001 (2021).

Biographies of the authors are not available.